lubricants

MDPI

Article

Inhomogeneous Nanoscale Conductivity and Friction on Graphite Terraces Explored via Atomic Force Microscopy

A. Kutay Ozyurt [1] and Mehmet Z. Baykara [2,*]

[1] Department of Materials Science and Engineering, University of California Merced, Merced, CA 95343, USA; aozyurt@ucmerced.edu
[2] Department of Mechanical Engineering, University of California Merced, Merced, CA 95343, USA
* Correspondence: mehmet.baykara@ucmerced.edu

Abstract: The interplay of conductivity and friction in layered materials such as graphite is an open area of investigation. Here, we measure local conductivity and friction on terraces of freshly cleaved highly oriented pyrolytic graphite via atomic force microscopy under ambient conditions. The graphite surface is found to exhibit a rich electrical landscape, with different terraces exhibiting different levels of conductivity. A peculiar dependency of conductivity on scan direction is observed on some terraces. The terraces that exhibit this dependency are also found to show enhanced friction values. A hypothesis based on tip asymmetry and the puckering effect is proposed to explain the findings. Our results highlight the non-triviality of the electrical and tribological properties of graphite on the nanoscale, as well as their interplay.

Keywords: atomic force microscopy; friction; graphite; nanoelectronics; nanotribology

check for updates

Citation: Ozyurt, A.K.; Baykara, M.Z. Inhomogeneous Nanoscale Conductivity and Friction on Graphite Terraces Explored via Atomic Force Microscopy. *Lubricants* **2024**, *12*, 462. https://doi.org/10.3390/lubricants12120462

Received: 13 November 2024
Revised: 16 December 2024
Accepted: 20 December 2024
Published: 21 December 2024

1. Introduction

Energy is an essential concept for humanity, closely intertwined with technological advancements. Even though our demand for energy is expected to accelerate in the future, conventional energy sources become increasingly unattractive due to environmental issues including climate change [1]. As the push for alternative, renewable energy sources continues [2], research efforts are also aimed at minimizing the "loss" of useful energy in mechanical systems. As such, tribology—the study of friction, wear, and lubrication—has become a vibrant field of research since the second half of the 20th century [3]. The accelerating progress in tribology research was spurred by the development of computational and experimental methods that have enabled the comprehension and harnessing of the complex physical phenomena that occur at the contact formed between sliding bodies [4].

The most conventional way to limit friction in mechanical systems is to use liquid lubricants [5]. Liquid lubricants are straightforward and convenient for use in numerous industrial and daily-life applications, playing a crucial role in enhancing the efficiency, durability, and performance of mechanical systems. On the other hand, there are specific conditions and applications for which the use of solid lubricants is required [6]. Solid lubricants are particularly important for (aero)space applications, where factors such as low temperatures and pressures render liquid lubricants ineffective [7,8]. Highly oriented pyrolytic graphite (HOPG) is one of the most well-known examples of solid lubricants [4]. The solid lubricating properties of HOPG are typically attributed to its layered (i.e., lamellar) structure, whereby individual sheets of carbon atoms held together by strong covalent bonds are stacked on top of each other, with sheets interacting with each other through weak van der Waals forces only. This anisotropic structure allows for easy sliding between the sheets, imparting to graphite its solid lubricating attributes. This scenario is specifically valid under humid conditions, where water and oxygen molecules passivate dangling bonds at the edges of individual sheets, which would otherwise lead to enhanced interactions between sheets and, thus, increase resistance to shear [9]. The high thermal

resistance of graphite also makes it valuable for certain high-temperature, tribological applications [10].

Recent advances in experimental methods have allowed the formation of a nanoscale understanding of tribological properties associated with solid lubricants. Within this context, the most prominent role belongs to the atomic force microscope (AFM) [11,12], which enables the recording of topographical maps as well as friction forces with sub-nanometer and sub-nanonewton resolution on material surfaces, effectively starting the field of "nanotribology" [13–15]. AFM can also be used to record the current flowing between the sharp AFM probe and a sample of interest under the application of a bias voltage with nanoscale spatial resolution; this mode of operation is commonly referred to as conductive atomic force microscopy (C-AFM) [16]. Recent work has revealed that the spatial resolution of C-AFM can reach the level of individual atoms, pushing the limits of this ever-developing method even further [17].

Understanding the nanoscale electronic properties of carbon-based materials such as HOPG [18] are important from a fundamental science point of view (especially considering the rise of two-dimensional materials in the last two decades, spurred on by the discovery of the extraordinary electronic properties of individual graphene sheets [19]). On the other hand, nanoscale conductivity, in general, is vital for developing technologies such nano-electromechanical systems (NEMs) [20], as well as microscale devices based on graphite [21]. For applications where tribological and electronic properties are central to functionality, such as triboelectric nanogenerators (TENGs) [22], AFM arises as a particularly useful tool with its capability of measuring both friction forces and currents with nanoscale spatial resolution. Despite this fact, studies focusing on combined/comparative experiments of nanoscale friction and conductivity performed via AFM are rather rare [23–25].

Motivated as above, we present here a combined study of nanoscale friction and conductivity on HOPG terraces, performed via AFM. Compared with previous C-AFM work performed on HOPG in the literature [18], our study stands out due to the simultaneous measurement of currents and friction at the tip–sample junction. Specifically, our findings reveal significant differences in conductivity and friction recorded on different terraces, and distinct differences in conductivity between forward (trace) and backward (retrace) scans, as well as changes in conductivity with normal load. Focusing on correlations between conductivity and friction, we propose potential physical mechanisms responsible for the observation of this rich landscape of nanoscale currents and friction forces encountered on the HOPG surface during AFM measurements.

2. Materials and Methods

The experiments were conducted under uncontrolled ambient conditions (temperatures of 30–35 °C and relative humidity levels of 30–40%) using a commercial AFM instrument (Asylum Research, Santa Barbara, CA, USA; Cypher VRS). It is important to note that fluctuations in temperature and humidity within these ranges were not found to affect the trends in conductivity and friction reported in Section 3. Mechanical exfoliation (i.e., cleaving via adhesive tape) was utilized to expose fresh surfaces of bulk HOPG crystals (Ted Pella, Redding, CA, USA; ZYB-quality) on which AFM experiments were performed. Two types of commercial, conductive cantilevers were utilized for the measurements: doped diamond-coated and Ti/Ir-coated (NanoSensors, Neuchatel, Switzerland; CDT-CONTR and Asylum Research, Santa Barbara, CA, USA; ASYELEC.01-R2, respectively), with normal spring constants of 0.6 ± 0.1 N/m and 2.5 ± 0.1 N/m, respectively. The normal calibration of the cantilevers was performed using the Sader method [26]. During the experiments, normal loads ranging from 0 nN to 20 nN were applied to the cantilevers. Mean adhesion forces were 16.4 nN and 6.1 nN, for doped diamond-coated and Ti/Ir-coated probes, respectively. The AFM measurements were carried out in contact mode, collecting lateral force signals along with topography and current maps. Bias voltages (V) ranging from 0 mV to 35 mV were applied between the sample and the AFM cantilever. The sizes of areas focused on during the measurements varied from 0.4×0.4 μm^2 to

$2.65 \times 2.65\ \mu m^2$. The scanning frequency was kept constant at 1 Hz. Friction force maps for each measurement were constructed from friction loops derived from the forward and backward lateral force signals [27]. This approach eliminates the influence of topography on measured lateral forces and provides absolute friction force values inherent to different regions of the sample surface.

Figure 1 provides a schematic of the combined AFM measurement approach, together with illustrative results. In particular, the AFM probe scans in forward and backward directions on areas of graphite that comprise terraces separated by step edges of various height, under the application of V. Results are collected simultaneously in the form of three maps (topography, current (I), and friction), allowing direct comparisons to be made between structural, electrical, and frictional characteristics.

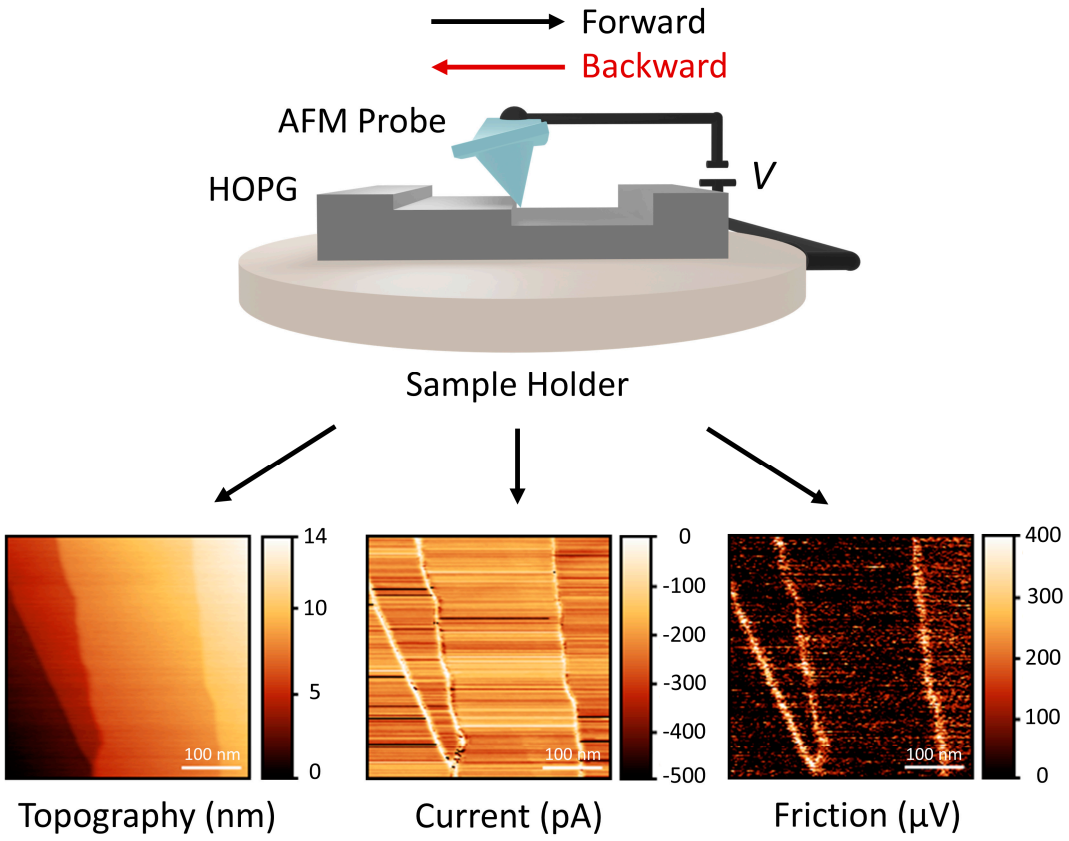

Figure 1. Schematic illustration of the AFM setup indicating the directions of forward and backward scans on the HOPG surface. The recorded outputs during AFM experiments include topography, current, and friction maps, representative examples of which are provided here. Please note that negative current values are reported due to a negative bias voltage being applied.

3. Results and Discussion

Figure 2 displays the results of two separate conductive AFM experiments performed on two different regions of graphite containing multiple terraces. In particular, Figure 2a,b depict current maps acquired during forward and backward scans, respectively, with clear differences in the conductivity landscape. Specifically, while some terraces exhibit similar conductivity values for both scan directions, the current values acquired on certain terraces are drastically different for forward and backward scans, with the most striking examples highlighted by black (forward) and red (backward) arrows in the current profiles depicted in Figure 2c. Current data acquired on another region of graphite, as depicted in Figure 2d,e, also result in the same conclusion, proving that the observed phenomenon (significant changes in conductivity on certain terraces as a result of scan direction) is not confined to a particular region on the sample surface.

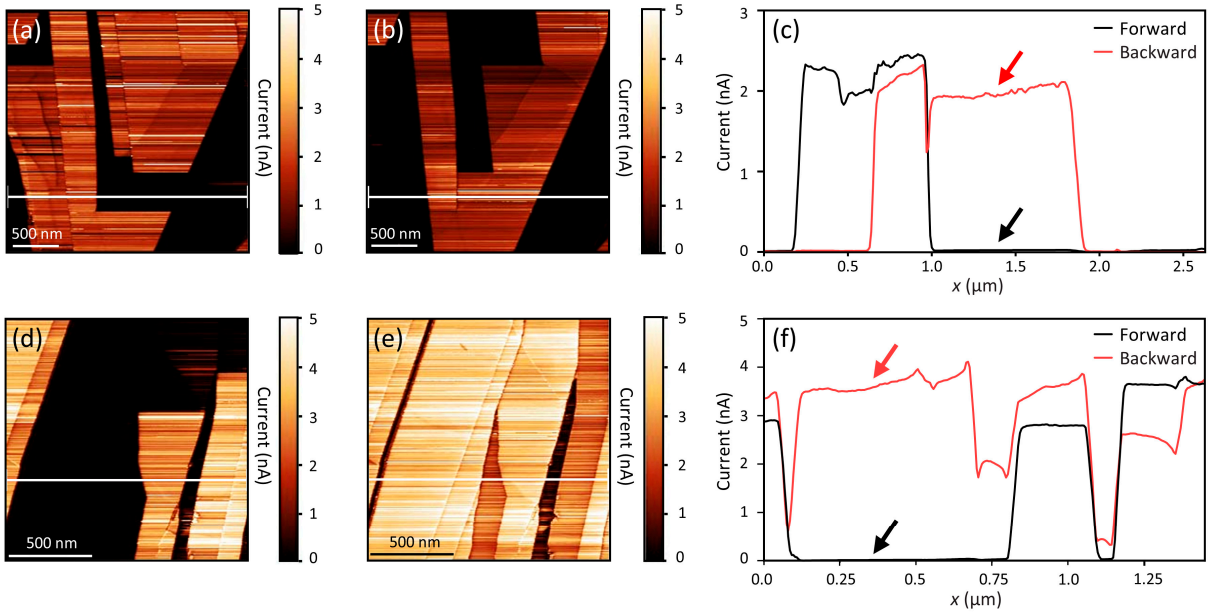

Figure 2. Quantitative analysis of conductivity differences on graphite terraces as a result of scan direction. (**a**,**b**) Current maps for forward and backward scans, respectively, illustrating variations in conductivity on graphite terraces. (**c**) Current profiles acquired along the white lines in (**a**,**b**), quantitatively confirming conductivity differences between forward (black) and backward (red) scans. (**d**,**e**) Current maps for forward and backward scans, respectively, acquired on another region of the graphite sample. (**f**) Current profiles acquired along the white lines in (**d**,**e**), quantitatively confirming conductivity differences between forward (black) and backward (red) scans. Arrows in (**c**,**f**) indicate representative regions on which stark conductivity differences are recorded as a function of scan direction. The bias voltage is 25 mV, while the applied normal load is zero. Data acquired with a doped diamond-coated probe.

In order to see if the prevalent conductivity differences on graphite terraces as a function of scan direction are accompanied by variations in frictional behavior, we performed combined experiments whereby current maps were recorded simultaneously with friction maps. Figure 3 presents representative results from such an experiment. Conductivity differences on certain graphite terraces in forward and backward scans are also observed in this experiment, as highlighted by the current maps shown in Figure 3a,b and the line profiles in Figure 3d. In particular, while the left- and right-most terraces (highlighted as I and IV in Figure 3a,b, respectively) exhibit similar conductivity values for both forward and backward scans, the two terraces in the middle (highlighted as II and III in Figure 3a,b) exhibit significant differences. The friction map recorded simultaneously with the current maps is depicted in Figure 3c. Interestingly, the two terraces that do show strong variations in conductivity as a function of scan direction (II and III) exhibit significantly enhanced (~3 times as much) friction when compared with terraces that do not exhibit strong direction dependence of conductivity (I and IV).

Complementing the comparative current and friction data presented in Figure 3, another data set of topography, current, and friction maps is presented in Figure 4. As observed in Figure 3, the two terraces that display the most drastic change in recorded current between forward (Figure 4b) and backward (Figure 4c) scans also exhibit enhanced friction values (Figure 4d) compared to the two other terraces where direction-dependent changes in current are much less significant.

To determine if the observed trends in conductivity are potentially affected by the pressure at the probe–sample contact, we repeated our experiments at different values of normal load. In particular, Figure 5 illustrates two sets of current maps and profiles recorded in forward and backward scanning directions, under applied normal load values of 0 nN (corresponding to adhesive contact, Figure 5a–c) and 20 nN (Figure 5d–f). While

the results shown in Figure 5a–c again demonstrate a strong direction dependency of conductivity (specifically for the middle terrace, highlighted as II), the application of a normal load of 20 nN results in an enhancement of current values on terraces I and II (Figure 5f). While this may initially appear as a suppression of the direction dependency effect when compared with the 0 nN normal load scenario, it needs to be taken into account that 20 nA represent the upper limit of current detectable with our AFM setup, thus leaving it an open question whether the recorded current values on terrace III would also have increased significantly with increasing normal load. Regardless, the effect of normal load on current values recorded on terraces I and II is clear.

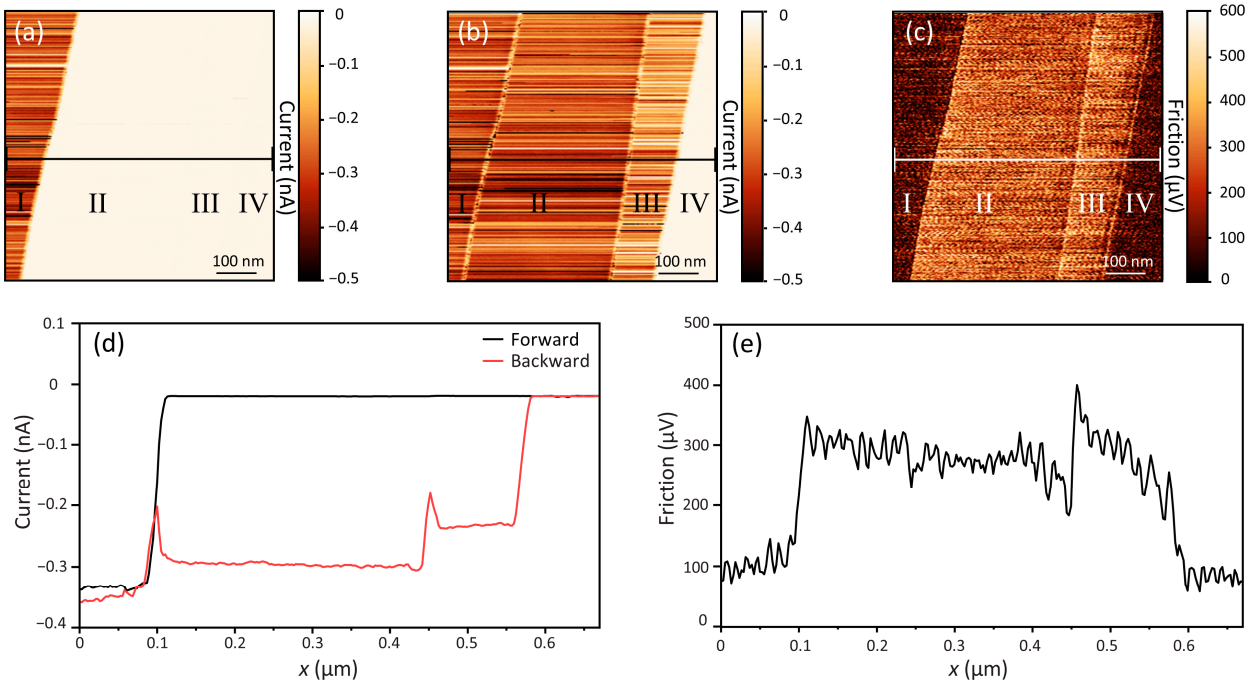

Figure 3. Comparative analysis of current and friction on graphite terraces I to IV. (**a**) Current map recorded during forward scan. (**b**) Current map on the same area, recorded during backward scan. (**c**) Simultaneously recorded friction map on the same area. (**d**) Current profiles acquired along the black lines in (**a**,**b**). (**e**) Friction profile acquired along the white line in (**c**), highlighting the enhanced friction encountered on terraces II and III. The bias voltage is 0 mV, while the applied normal load is zero. Data acquired with a doped diamond-coated probe.

It is important to note that the conductivity variations on different graphite terraces exemplified by the representative results in Figures 2–5 as a function of scan direction were universally observed during our measurements, after multiple (3) cleaves of the graphite sample, tested with multiple (two Ti/Ir-coated and four doped diamond-coated) AFM probes. As such, it is not possible to assign the physical mechanism behind the observations to specific properties of the investigated sample regions or specific tip asymmetry effects alone. Additionally, the fact that only certain terraces exhibit a strong direction dependency of conductivity on scanning direction, while others appear similar or exhibit comparatively minor differences indicates that certain regions/terraces on the cleaved graphite surface are inherently different compared to the other ones. In order to hypothesize about the physical reasons behind our observations, we turn to previous C-AFM work performed on HOPG. In particular, Banerjee et al. observed distinct differences in conductivity on different graphite terraces on HOPG in their C-AFM measurements, where the direction dependence of conductivity measurements was not studied [18]. The reason behind the observed differences in conductivity between different terraces (or alternatively, "ribbons/strips" of graphite) was attributed to the mechanical cleaving process; specifically, it was argued that exfoliation via adhesive tape led to vertical and/or lateral displacement (i.e., dislodgement)

of certain regions in the upper layers of the graphite substrate, which in turn led to variations in electrical conductivity due to altered interactions with the bulk [18]. As already illustrated in detail, in our measurements, we additionally observed that certain terraces exhibited differences in electrical conductivity as a function of scanning direction. The availability of friction force as an additional data channel provides clues with regard to the physical origins of this behavior. Specifically, as illustrated in Figures 3 and 4, we repeatedly observed that terraces exhibiting strong direction dependence of conductivity also exhibited enhanced friction forces. The variation in friction on layered materials such as graphite as a function of number of layers has been studied extensively via AFM and attributed to the "puckering" phenomenon [28]. Puckering involves the idea that individual layers of a material such as graphite exhibit increased friction during AFM measurements when compared with multiple layers, due to vertical deformations around the sharp AFM probe that effectively wrap the material around it, thus increasing friction values. This effect diminishes for the bulk versions of the material as the increasing bending stiffness suppresses the vertical deformations. Based on this information, one can argue that those regions of the graphite surface that exhibit strong direction dependence of current are those terraces/ribbons that have been dislodged sufficiently from the bulk, thus exhibiting the puckering effect, which manifests as enhanced friction.

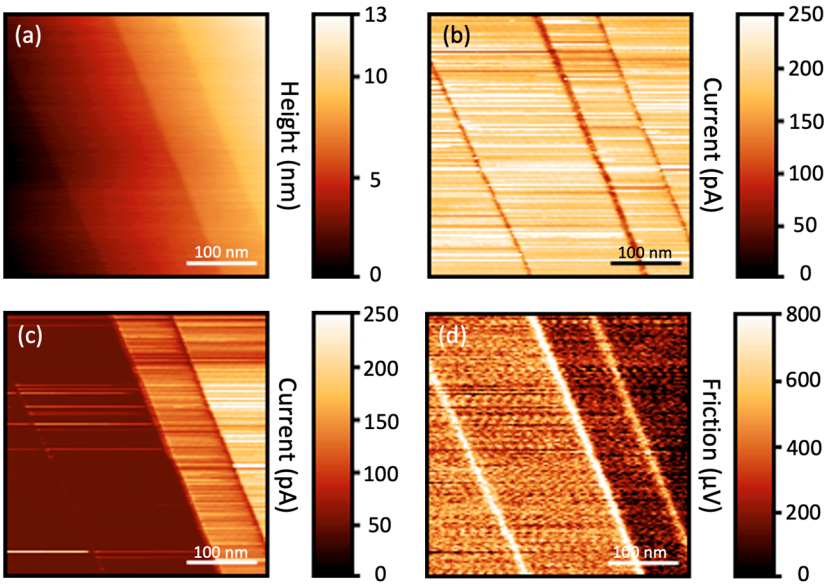

Figure 4. Comparative analysis of current and friction on four graphite terraces. (**a**) Topography map recorded during forward scan. (**b**) Current map recorded during forward scan. (**c**) Current map on the same area, recorded during backward scan. (**d**) Simultaneously recorded friction map on the same area, highlighting enhanced friction on the two terraces on the left. The bias voltage is 10 mV, while the applied normal load is zero. Data acquired with a doped diamond-coated probe.

The remaining question is then why different values of conductivity are measured on these dislodged regions when they are scanned in opposite directions (forward vs. backward). In order to answer this question, it is important to realize that AFM probe apexes are almost always structurally asymmetric, and the degree to which this asymmetry affects measurements depends on how much of the vertical extent of the probe is involved in the measured interactions [29]. As such, it is conceivable that the degree of puckering on dislodged terraces/regions (and consequently, the effective contact area) could be significantly different for AFM probes scanning in one direction vs. the other, depending on the structural asymmetry of the probe apex. Therefore, scans in one direction could result in larger contact areas (and therefore, higher currents) while the inverse would be true for the other direction. On terraces/ribbons that are not dislodged from the bulk, the effect of tip asymmetry on the direction dependence of current would be minimal (but

potentially still observable, as is the case for the right-most two terraces in Figure 4), as puckering does not take place, and only a limited region of the tip apex interacts with the substrate. Having said this, it needs to be acknowledged that the experimental verification of this scenario remains difficult. The main reason for this is that while scanning electron microscopy (SEM) can be used to observe tip apexes on the scale of several nanometers [30], and transmission electron microscopy (TEM) can provide atomic-resolution spatial detail on tip apex structures [31], (i) these characteristics change as soon as the tip makes contact with the sample, and (ii) only a very small, specific portion of the tip apex interacts with the sample surface. Therefore, evaluation of tip asymmetry for individual experiments remains challenging.

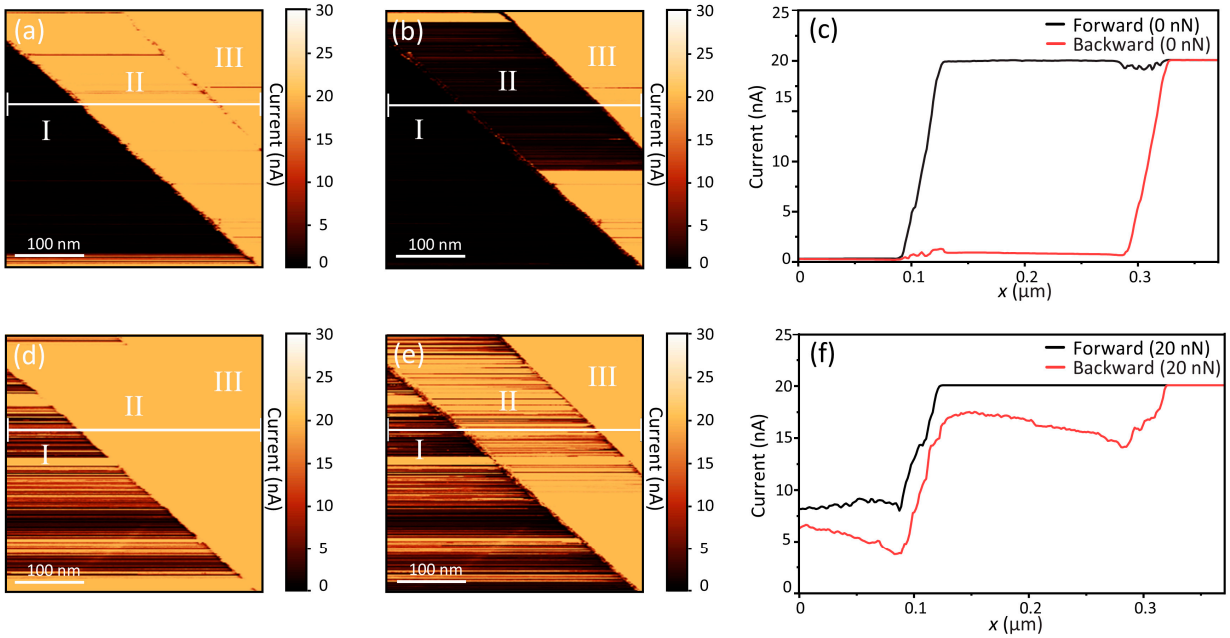

Figure 5. Quantitative analysis of conductivity differences on graphite terraces I to III as a function of scan direction and normal load. (**a**,**b**) Current maps for forward and backward scans, respectively, recorded under a normal load of 0 nN. (**c**) Current profiles acquired along the white lines in (**a**,**b**). Current maps for forward and backward scans, respectively, recorded under a normal load of 20 nN. (**f**) Current profiles acquired along the white lines in (**d**,**e**), showing an increase in current values recorded in the backward scan direction. The bias voltage is 1 mV. Data acquired with a Ti/Ir-coated probe.

Despite the apparent self-consistency of the hypotheses above, certain open questions remain from the presentation of our results. In particular, while Figure 5 demonstrates that current values recorded on terraces indeed increased with the application of normal load (which may simply have occurred due to the increase in contact area) [32], the question of whether normal loads can suppress the direction dependency of current remains. Additionally, as one can see in Figure 5b, only a certain region on terrace II exhibited direction dependency of current while the rest did not. The observation that the boundaries of this region aligned perfectly with the horizontal scanning direction of the AFM probe could lead to the impression that temporary tip changes are the reason behind the diminished current. On the other hand, the confinement of the effect to a single terrace disproves this notion. An alternative explanation could involve a scenario where the probe damages/exfoliates the terrace in question [33]. Such alternative scenarios, however, need validation through complementary computational work.

4. Conclusions

In conclusion, we presented results of combined conductivity and friction measurements on graphite, performed via AFM. A strong dependence of conductivity on scanning direction was observed on certain terraces, which were also found to exhibit enhanced friction forces. A physical picture involving the dislodgement of such terraces from the bulk substrate during the mechanical exfoliation process potentially explains the observed trends, whereby the combination of puckering and tip asymmetry could lead to the direction dependence of measured current values. On the other hand, the experimental verification of this hypothesis remains difficult due to limitations associated with the structural characterization of tip apexes on the nanometer scale and the inability to observe the tip–sample contact region in situ during sliding. As such, future work involving computational approaches would certainly be needed to verify and/or revise the hypotheses. Regardless of the hypotheses presented here, the experimental results unequivocally demonstrate the non-triviality of nanoscale conductivity and friction on graphite, with implications for device designs where the interplay of electrical and tribological phenomena are central to functionality.

Author Contributions: A.K.O.: formal analysis, investigation, methodology, validation, writing—original draft, and writing—review and editing. M.Z.B.: conceptualization, supervision, and writing—review and editing. All authors have read and agreed to the published version of the manuscript.

Funding: This research was funded by the National Science Foundation (NSF) via Award No. 2131976.

Data Availability Statement: The raw data supporting the conclusions of this article will be made available by the authors on request.

Conflicts of Interest: The authors declare no conflicts of interest.

References

1. VijayaVenkataRaman, S.; Iniyan, S.; Goic, R. A review of climate change, mitigation and adaptation. *Renew. Sustain. Energy Rev.* **2012**, *16*, 878–897. [CrossRef]
2. Gielen, D.; Boshell, F.; Saygin, D.; Bazilian, M.D.; Wagner, N.; Gorini, R. The role of renewable energy in the global energy transformation. *Energy Strategy Rev.* **2019**, *24*, 38–50. [CrossRef]
3. Jost, H.P. Tribology—Origin and future. *Wear* **1990**, *136*, 1–17. [CrossRef]
4. Bhushan, B. *Introduction to Tribology*; Wiley: New York, NY, USA, 2013.
5. Mang, T.; Bobzin, K.; Bartels, T. *Industrial Tribology: Tribosystems, Friction, Wear and Surface Engineering*; Wiley: Weinheim, Germany, 2011.
6. Donnet, C.; Erdemir, A. Historical developments and new trends in tribological and solid lubricant coatings. *Surf. Coat. Technol.* **2004**, *180–181*, 76–84. [CrossRef]
7. Roberts, E. Thin solid lubricant films in space. *Tribol. Int.* **1990**, *23*, 95–104. [CrossRef]
8. Roberts, E.W. Space tribology: Its role in spacecraft mechanisms. *J. Phys. D Appl. Phys.* **2012**, *45*, 503001. [CrossRef]
9. Scharf, T.W.; Prasad, S.V. Solid lubricants: A review. *J. Mater. Sci.* **2013**, *48*, 511–531. [CrossRef]
10. Sliney, H.E. Solid lubricant materials for high temperatures—A review. *Tribol. Int.* **1982**, *15*, 303–315. [CrossRef]
11. Binnig, G.; Quate, C.F.; Gerber, C. Atomic force microscope. *Phys. Rev. Lett.* **1986**, *56*, 930–933. [CrossRef]
12. Mate, C.M.; McClelland, G.M.; Erlandsson, R.; Chiang, S. Atomic-scale friction of a tungsten tip on a graphite surface. *Phys. Rev. Lett.* **1987**, *59*, 226–229. [CrossRef] [PubMed]
13. Bhushan, B.; Israelachvili, J.N.; Landman, U. Nanotribology: Friction, wear and lubrication at the atomic scale. *Nature* **1995**, *374*, 607–616. [CrossRef]
14. Bhushan, B. *Nanotribology and Nanomechanics: An Introduction*; Springer: Berlin/Heidelberg, Germany, 2008.
15. Gnecco, E.; Meyer, E. *Fundamentals of Friction and Wear*; Springer: Berlin/Heidelberg, Germany, 2007.
16. Murrell, M.P.; Welland, M.E.; O'Shea, S.J.; Wong, T.M.H.; Barnes, J.R.; McKinnon, A.W.; Heyns, M.; Verhaverbeke, S. Spatially resolved electrical measurements of SiO_2 gate oxides using atomic force microscopy. *Appl. Phys. Lett.* **1993**, *62*, 786–788. [CrossRef]
17. Sumaiya, S.A.; Liu, J.; Baykara, M.Z. True atomic-resolution surface imaging and manipulation under ambient conditions via conductive atomic force microscopy. *ACS Nano* **2022**, *16*, 20086–20093. [CrossRef]
18. Banerjee, S.; Sardar, M.; Gayathri, N.; Tyagi, A.K.; Raj, B. Conductivity landscape of highly oriented pyrolytic graphite surfaces containing ribbons and edges. *Phys. Rev. B* **2005**, *72*, 075418. [CrossRef]
19. Novoselov, K.S.; Geim, A.K.; Morozov, S.V.; Jiang, D.; Zhang, Y.; Dubonos, S.V.; Grigorieva, I.V.; Firsov, A.A. Electric field effect in atomically thin carbon films. *Science* **2004**, *306*, 666–669. [CrossRef]
20. Craighead, H.G. Nanoelectromechanical systems. *Science* **2000**, *290*, 1532–1535. [CrossRef] [PubMed]

21. Wu, T.; Chen, W.; Wangye, L.; Wang, Y.; Wu, Z.; Ma, M.; Zheng, Q. Ultrahigh critical current density across sliding electrical contacts in structural superlubric state. *Phys. Rev. Lett.* **2024**, *132*, 096201. [CrossRef] [PubMed]
22. Fan, F.-R.; Tian, Z.-Q.; Wang, Z.L. Flexible triboelectric generator. *Nano Energy* **2012**, *1*, 328–334. [CrossRef]
23. Enachescu, M.; Schleef, D.; Ogletree, D.F.; Salmeron, M. Integration of point-contact microscopy and atomic-force microscopy: Application to characterization of graphite/Pt (111). *Phys. Rev. B* **1999**, *60*, 16913–16919. [CrossRef]
24. Nowakowski, K.; Zandvliet, H.J.W.; Bampoulis, P. Barrier inhomogeneities in atomic contacts on WS_2. *Nano Lett.* **2018**, *19*, 1190–1196. [CrossRef] [PubMed]
25. Chan, N.; Vazirisereshk, M.R.; Martini, A.; Egberts, P. Insights into dynamic sliding contacts from conductive atomic force microscopy. *Nanoscale Adv.* **2020**, *2*, 4117–4124. [CrossRef] [PubMed]
26. Sader, J.E.; Chon, J.W.M.; Mulvaney, P. Calibration of rectangular atomic force microscope cantilevers. *Rev. Sci. Instrum.* **1999**, *70*, 3967–3969. [CrossRef]
27. Schwarz, U.D.; Köster, P.; Wiesendanger, R. Quantitative analysis of lateral force microscopy experiments. *Rev. Sci. Instrum.* **1996**, *67*, 2560–2567. [CrossRef]
28. Lee, C.; Li, Q.; Kalb, W.; Liu, X.-Z.; Berger, H.; Carpick, R.W.; Hone, J. Frictional characteristics of atomically thin sheets. *Science* **2010**, *328*, 76–80. [CrossRef] [PubMed]
29. Uluutku, B.; Baykara, M.Z. Artifacts related to tip asymmetry in high-resolution atomic force microscopy and scanning tunneling microscopy measurements of graphitic surfaces. *J. Vac. Sci. Technol. B* **2015**, *33*, 031802. [CrossRef]
30. Demirbaş, T.; Baykara, M.Z. Nanoscale tribology of graphene grown by chemical vapor deposition and transferred onto silicon oxide substrates. *J. Mater. Res.* **2016**, *31*, 1914–1923. [CrossRef]
31. Jacobs, T.D.B.; Carpick, R.W. Nanoscale wear as a stress-assisted chemical reaction. *Nat. Nanotechnol.* **2013**, *8*, 108–112. [CrossRef] [PubMed]
32. Sumaiya, S.A.; Martini, A.; Baykara, M.Z. Improving the reliability of conductive atomic force microscopy-based electrical contact resistance measurements. *Nano Express* **2020**, *1*, 030023. [CrossRef]
33. Özoğul, A.; Gnecco, E.; Baykara, M.Z. Nanolithography-induced exfoliation of layered materials. *Appl. Surf. Sci. Adv.* **2021**, *6*, 100146. [CrossRef]